Direct visualization of relativistic Coulomb field in the near and far field ranges

To cite this article before publication: Mario Galletti *et al* 2023 *New J. Phys.* in press https://doi.org/10.1088/1367-2630/acdbe4

Direct visualization of relativistic Coulomb field in the near and far field ranges

M. Galletti,[1, 2, 3, *] A. Cianchi,[1, 2, 3] A. Curcio,[4] F. Dipace,[5] M. Ferrario,[5] and R. Pompili[5]

[1] *Department of Physics, Università di Roma Tor Vergata, Via Ricerca Scientifica 1, 00133 Rome, Italy*
[2] *INFN-Tor Vergata, Via Ricerca Scientifica 1, 00133 Rome, Italy*
[3] *Nast Center, Via Ricerca Scientifica 1, 00133 Rome, Italy*
[4] *Centro de Laseres Pulsados (CLPU), Parque Cientifico, 37185 Villamayor, Salamanca, Spain*
[5] *Laboratori Nazionali di Frascati, Via Enrico Fermi 54, 00044 Frascati, Italy*

(Dated: May 26, 2023)

Coherent emission coming from relativistic charged bunches is of great interest in a wide range of user-oriented applications and high-resolution diagnostics. The complete characterization of such emission is therefore important in view of a complete understanding of its potential. Here we present a complete temporally-resolved characterization of the radiation emitted by ultra-short relativistic electron bunches using a temporal diagnostic based on Electro-Optical Sampling with a few tens fs of temporal resolution. We have characterized, for the first time to our knowledge, the evolution of the radiation (in THz range) both in amplitude and direction of propagation by varying the detection (i.e., the observer) position from the near to the far field range. Results show that in the near-field regime the emitted radiation propagates collinearly with the electron beam; while, approaching the far-field regime, the radiation behaves as the classical Cherenkov radiation.

In the last few decades, great interest has been shown in coherent radiation produced by ultra-short electron bunches with femtosecond durations. The radiation is emitted as an ultra-short pulse in the millimeter and sub-millimeter (THz) range and can be adopted in a wide range of scientific areas. It can be employed to directly probe the microscopic structure of matter [1, 2] or as a diagnostic of the bunch itself, for instance, to retrieve its longitudinal charge profile [3–6].

The usual picture to describe the radiation emission process is to start from the electromagnetic wave generated by a single charged particle, as formulated by Lienard and Wiechert. According to this theory, the emitted electromagnetic field is radiated when a charged particle undergoes acceleration [7], meaning a variation of its velocity due to an external field, or crosses the boundary between two different media [8]. This approach can be used to describe all the main formation mechanisms for synchrotron, transition, diffraction and Vavilov-Cherenkov radiations [9–14]. The radiation field is composed of two terms [7, 15], (i) the *near-field* (NF), falling as the square of the distance and well-known as the Coulomb field for a particle at rest and (ii) the *far-field* (FF), scaling as the inverse of the distance for accelerated charges. In many works the far-field term ($\propto \mathbf{r}^{-1}$) is the only one that is considered since the observer is usually considered to be far from the radiation formation region. But when the detector is located near the emitting bunch, the near-field term ($\propto \mathbf{r}^{-2}$) should definitely be included since its effect becomes dominant.

In this work, we present experimental results showing the temporally-resolved characterization of the THz radiation emitted by an ultra-short relativistic electron bunch. The detection of the radiation is performed using a temporal diagnostic based on Electro-Optical Sampling (EOS) [16]. The experiment has been carried out at the SPARC_LAB test-facility [17] by employing the electron bunches produced by the high-brightness SPARC photo-injector [18, 19]. We have characterized, for the first time to our knowledge, the evolution of the THz radiation features, namely its amplitude and duration, in the near- to the far-field observation regimes [20]. We observe, in the far-field limit, that radiation moves along the Cherenkov angle, typical of the Vavilov-Cherenkov Radiation (VCR); on the contrary, in the near-field limit, the pattern of the radiation is dominated by near-field effects and leads to a radiation front propagating collinearly with the radiating electron bunch. The results have been compared with previous theoretical models [21], showing an excellent agreement.

The experimental setup is shown in Fig. 1. An ultra-short electron bunch is produced by the SPARC_LAB photo-injector [22], consisting of a radio-frequency (RF) gun providing a 120 MV/m peak electric field followed by three accelerating sections. The bunches are generated by sending UV pulses, whose shape and duration can be tailored according to the experimental task, directly on the metallic Cu cathode [23] and are longitudinally compressed by the photo-injector down to a few tens of femtosecond durations [24]. The beam diagnostics consist of an EOS station able to monitor the bunch features in a non-intercepting and single-shot way. The EOS is based on the spatial encoding technique [25] and its temporal resolution is estimated to be of the order of 50 fs [26]. The beam diagnostics is completed by an RF-Deflector and a magnetic spectrometer allowing to characterize the time and energy profiles of the beam in correspondence of a cerium-doped yttrium aluminium garnet (Ce:YAG) screen located on a 14° beamline [27]. Beam current monitors installed along the machine allow us to measure the beam charge at different locations.

The SPARC photo-injector is capable to produce dif-

ferent beam configurations according to the experimental campaigns. For the purposes of this work, we tuned the longitudinal compressor to produce 200 pC bunches with $\approx$ 150 fs temporal duration. The beam energy was varied in the range 37-96 MeV. The EOS diagnostics consists of 200 μm thick ZnTe and 100 μm thick GaP crystals. The electron beam propagates at distances in the range of $0.15 - 2.5$ mm from the side of the EOS crystals, as shown in Fig.1. The EOS relies on a ≈ 100 fs probe IR laser, directly split from the photo-cathode laser system, ensuring a jitter-free synchronization. The laser impinges the crystal at 30° incidence angle, providing an effective temporal window of $\approx$ 10 ps. The EOS setup is completed by a lens ($f = 30$ cm) installed downstream of the crystal and used to image the crystal surface on the CCD camera where the EOS signals are actually recorded. In such a way we can assume the crystal itself as the effective position of the observer. The temporal overlap of the radiation produced by the emitting electrons and probe laser in correspondence with the EOS crystal is obtained by a 3 fs resolution delay-line on the probe path.

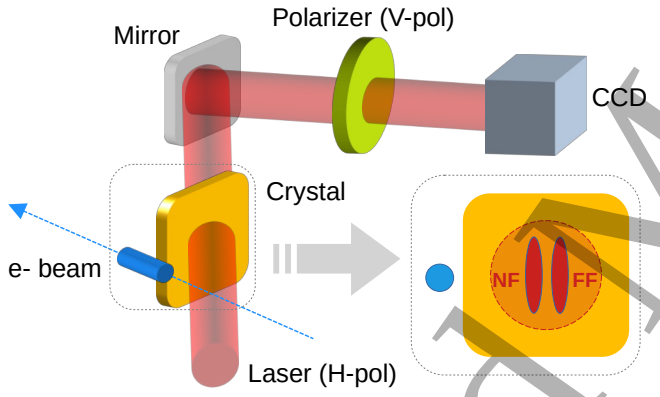

Figure 1. Setup of the experiment. The horizontally polarized IR laser crosses the crystal with 30° incidence angle. The electron beam travels near the crystal, inducing the electro-optic effect that rotates the laser polarization. The position of the electron beam with respect to the crystal is adjusted with a magnetic steerer located upstream. The modulation of the laser polarization is then converted into an intensity modulation by means of a polarizer whose axis is orthogonal to the initial laser polarization. The modulated laser transverse profile is then imaged onto a CCD camera. The inset shows the location of the near-field (NF) and far-field (FF) areas.

To figure out how the detection is performed, Fig. 2 shows three recorded EOS snapshots related to an electron bunch with a temporal duration of 150 fs and an energy of 96 MeV at several positions R with respect to the EOS crystal (i.e., the observation point of view). The detected EOS signals are able to give information both on the electron bunch properties and on its irradiated field. The electric field (Σ_e) and the temporal duration (τ_e) of the emitting electron bunches can be retrieved from the signal amplitude and width [28], respectively. Concurrently, the experimental traces allow us to fully characterize the radiation, namely its amplitude and propagation angle, both depending on the observation regime (near- or far-field, according to the well-known Lienard-Wiechert theory). When moving toward the far-field limit (i.e. growing distance R from crystal), it is noticeable the appearance of an additional signal. When the distance is as large as $R \rightarrow 3$ mm, the additional signal related to the far-field signal increases its amplitude. On the contrary, the near-field signal amplitude is depleting.

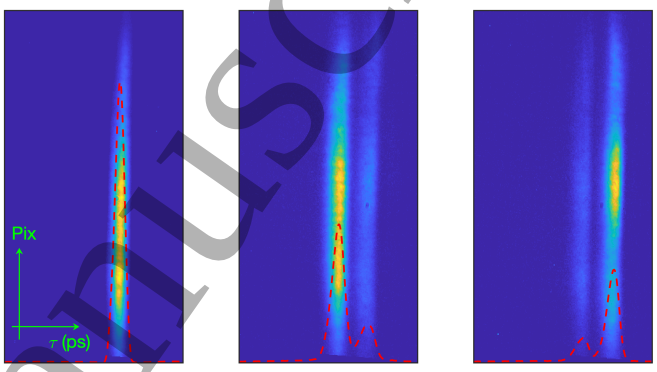

Figure 2. **Detected EOS signal** The radiation of an electron bunch with a temporal duration of $\tau_e \sim 150$ fs and energy of $E_e \sim 96$ MeV for different positions R (R is the distance between the EOS crystal edge and the electron bunch axis) with respect to the observer, namely R $\approx 0.15, 1, 2$ mm. R $\rightarrow$ 0.15 mm detection in the near-field regime; while, R $\rightarrow$ 3 mm detection in the far-field regime. The x-axis represents the longitudinal propagation of the signal, the y-axis is the pixel number. The color scale is renormalized for each position R; while, the lineout of the raw correspondent snapshots represents the intensity of the signals. Increasing R, it shows the evolution of the electric field: depletion of the near-field and growth od the far-field.

Figure 2 also shows tat the two signals appear delayed in time and this corresponds to two non co-propagating beams along the EOS crystal. It is straightforward to determine the propagation angle of the far-field signal, considering the distance between the two signals (L_s, namely the distance between the two peaks shown in Fig.2) and the crystal thickness (L_c)

$$\theta(R) = 90° - \arctan\left[\frac{L_s}{L_c}\right] \quad (1)$$

As mentioned before, we have adopted both high and low energy electron bunches to show the features of the radiation in the near and far-field limits. Adopting Eq.1, Fig.3 was sorted out. It shows the experimental results regarding the effective propagation angle as a function of the observation distance for the four different bunch energies. In the case $E = 96$ MeV and the distance from R = 0.15 mm to R $\rightarrow$ 0.7 mm, we get $\theta < 7^o$,

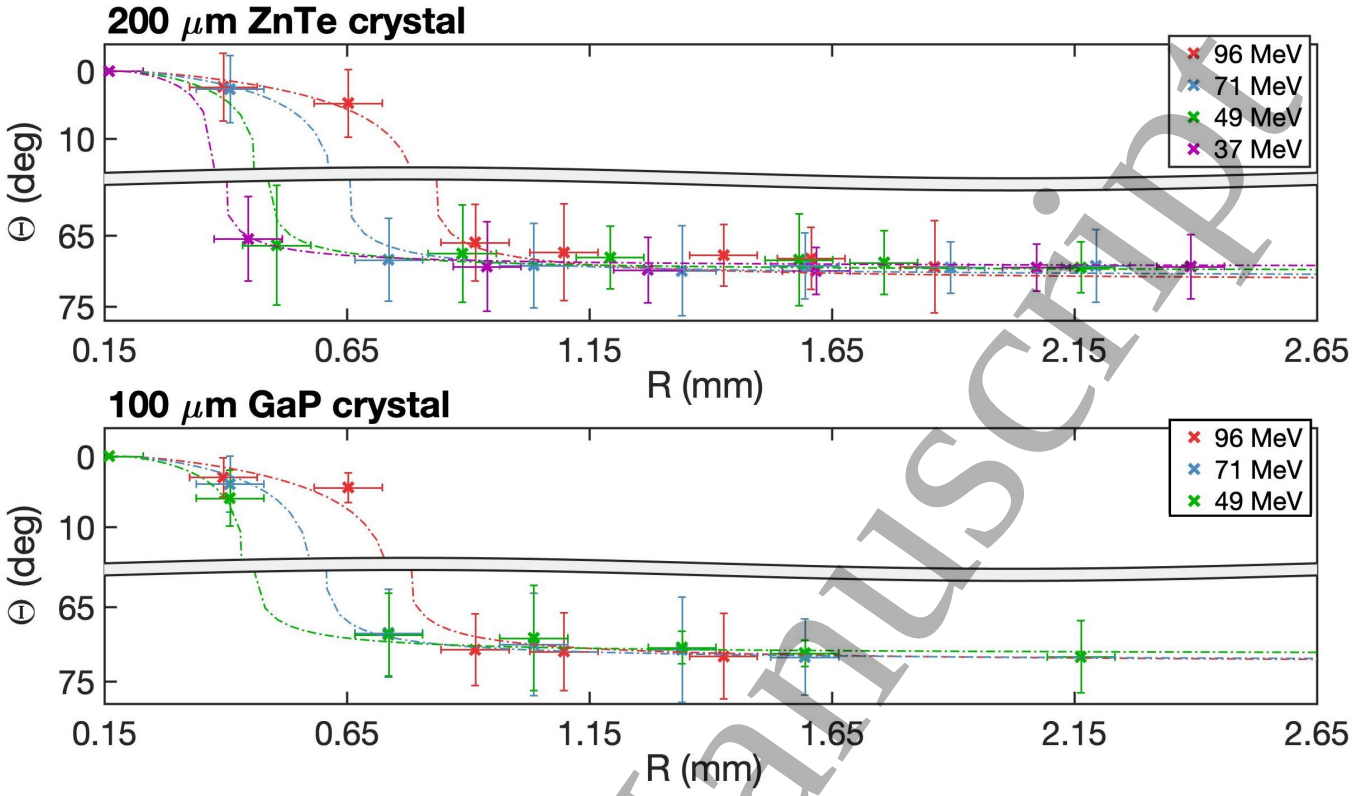

Figure 3. **Experimental Data** Effective Cherenkov angle, associated with the emitting ultrafast electron bunches for four different energies, as a function of the observation distance. The set of data (coloured crosses) was taken for two different EOS crystal a 200 μm ZnTe (n_{ZnTe} ~3) and a 100 μm GaP (n_{GaP} ~3). The theoretical curves (dashed coloured lines) were calculated with Eq.2.

indicating a radiation front propagating almost parallel to the bunch propagation direction. On the contrary, for the same energy but the distance from $R \sim 0.7$ mm to R $\rightarrow$ 3 mm, we get $\theta \sim 70^o$, close to the classical Cherenkov angle value $\theta_c = \arccos(1/n\beta_0) \sim 72^o$. Moreover, it is noticeable that the near-field range decreases (far-field range increases) decreasing the electron bunch energy ($E = 71 \rightarrow 37$ MeV) according to the theory developed in Ref. [21]. This non-collinear behaviour of the radiation is consistent for all the beam energies and by using two electro-optic crystals (i.e., different indexes of refraction) with different thicknesses as shown in Fig.3. Indeed, considering the retrieved properties of the electron bunches, the radiation wavelength $\lambda_{THz} = 30\mu m$, the indexes of refraction of the ZnTe and GaP crystals in our THz range n_{ZnTe} ~3 and n_{GaP} ~3, we calculated the effective propagation angle of the emitted radiation as [21]

$$\theta_{th}(R) = \arccos\left[\frac{\bar{p}_z}{\sqrt{\bar{p}_z^2 + \bar{p}_r^2}}\right] \qquad (2)$$

where $\bar{p}_{r,z}$ are the average radial and longitudinal momenta of the electromagnetic field. It is worth to notice that here we use a definition of angle which is complementary to the one in Ref. [21], since this choice is more in line with standard notation for the Cherenkov angle. The momenta are given by $\bar{p}_{r,z} = N_{r,z}\hbar\bar{k}_{r,z}$, where $N_{r,z}$ is the number of photons and $\hbar\bar{k}_{r,z}$ their average momentum.

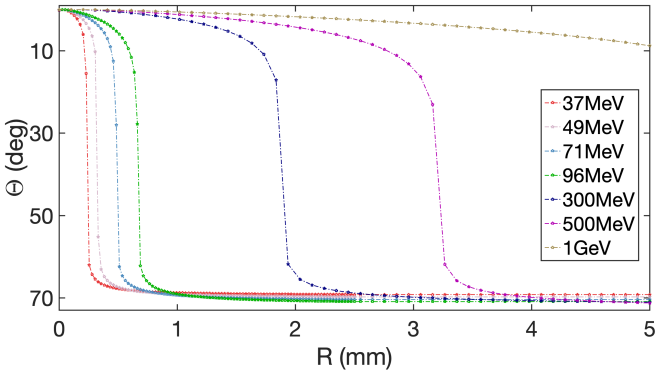

Figure 4. **Theoretical Data** Theoretical curves regarding the effective Cherenkov angle, associated with the emitting ultrafast electron bunches for different energies, as a function of the observation distance. The set of data was calculated for a 200 μm ZnTe (n_{ZnTe} ~3) EOS crystal adopting Eq.2.

Eq.2 converges to the classical Cherenkov angle in the far-field limit, as mentioned before, with the effective Cherenkov angle increasing when decreasing the electron bunch energy. The analytical calculations are also reported in Fig.4 showing an excellent agreement with the experimental data reported in Fig.3.

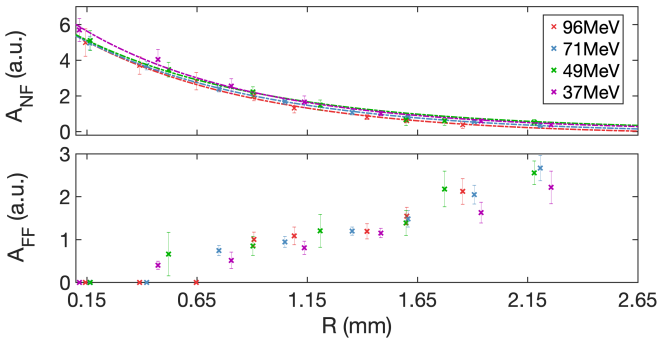

Figure 5. **Experimental Data** (Up) EOS NF signal amplitude, associated with the emitting ultrafast electron bunches with four different energies, as a function of the observation distance. The set of data (coloured crosses) was taken for the 200 μm ZnTe EOS crystal. The theoretical fits (dashed coloured lines) were calculated with Eq.3. (Down) EOS FF signal amplitude, associated with the emitting ultrafast electron bunches with four different energies, as a function of the observation distance. The set of data (coloured crosses) was taken for the 200 μm ZnTe EOS crystal. A linear behaviour of the amplitude is shown.

Finally, to fully characterize the THz radiation, we studied the amplitude of the NF component, the experimental behaviour of the FF amplitude component and of the temporal duration of both signals as a function of the R parameter with respect to the energy of the emitting relativistic electron bunches. The space-charge field for a gaussian beam can be written as follows

$$\Sigma_{THz} \propto A_{NF_0} \frac{(1-\exp\frac{R^2}{2\sigma^2})}{R} \qquad (3)$$

where σ is the electron beam radius. Adopting Eq.3, we were able to fit the experimental data regarding the NF amplitude of the emitted THz field as a function of the observation distance for the four different bunch energies, as shown in Fig.5,(Up). The fit parameters are reported in Table I.

E(MeV)	$\mathbf{A}_{NF_0}$**(a.u.)**
96	2.6±0.4
71	2.4±0.3
49	2.8±0.4
37	2.7±0.4

Table I. **Theoretical analysis** Fitting the experimental data with Eq.3, the amplitude of each electric field component was retrieved.

Considering the retrieved fit parameter A_{NF_0}, we measure that the radiation field is independent of the electron bunch energy in our experimental conditions. In Fig.5,(bottom), the experimental behaviour of the FF radiation amplitude is shown. A linear growth is retrieved in the spatial range of interest. Finally, the temporal duration of both signals was retrieved as a function of the observation distance. As shown in Fig.6, the duration of the NF signal is constant ($\sim$ 150 fs) within the studied range, meanwhile, the FF signal duration grows almost linearly from $\sim$ 160 fs to $\sim$ 250 fs at the furthest point. In the NF, the duration of the signal corresponds to the one of the electron bunch because the diagnostic system is not cutting any spectral bandwidth for $R \lesssim \gamma\beta\lambda/2\pi$. Meanwhile, going towards the furthest position $R \gtrsim \gamma\beta\lambda/2\pi$, the NF signal is depleted and the FF signal is enhanced and stretched because of the cutting of the high frequencies in the spectral bandwidth. In our experimental campaign, $\gamma\lambda/2\pi$ is in the mm range. It is noticeable, as shown in Fig.6, that the maximum temporal duration is reached sooner by the lower energy electron bunches because they cut high frequencies for lower distances.

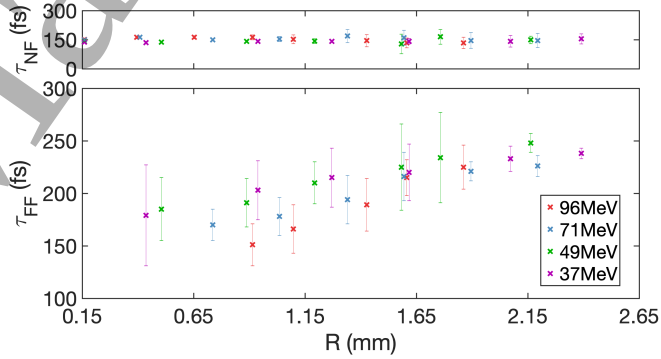

Figure 6. **Experimental Data** EOS NF signal (Up) and FF signal (Down) duration, associated with the emitting ultrafast electron bunches with four different energies, as a function of the observation distance. The set of data (coloured crosses) was taken for the 200 μm ZnTe EOS crystal. A linear behaviour of the amplitude is shown.

In conclusion, we have presented direct temporally-resolved sub-picosecond resolution measurements of the radiation emitted by relativistic electron bunches. According to the electron energy ($37-96$ MeV range) and the distance ($0.15-2.5$ mm range) between the electron bunch and the EOS diagnostic, the radiation can be considered in the near-field of the Vavilov-Cherenkov radiation, i.e. where the field is similar to a point charge field propagating collinearly to the emitting bunch, or in the far-field, where the radiation propagates at the well-known Cherenkov angle $\arccos(1/\beta_0 n)$. Analytic calculations were performed to validate the behaviour experimentally retrieved. The results provide a more complete

picture of the radiation process emission, underlying its formation mechanism.

ACKNOWLEDGMENTS

This work has been partially supported by the EU Commission in the Seventh Framework Program, Grant Agreement 312453−EuCARD−2, the European Union Horizon 2020 research and innovation program, Grant Agreement No. 653782 (EuPRAXIA) and the INFN with the GRANT73/PLADIP grant.

* mario.galletti@lnf.infn.it

[1] Z. Wu, A. S. Fisher, J. Goodfellow, M. Fuchs, D. Daranciang, M. Hogan, H. Loos, and A. Lindenberg, Review of Scientific Instruments **84**, 022701 (2013).

[2] F. Giorgianni, E. Chiadroni, A. Rovere, M. Cestelli-Guidi, A. Perucchi, M. Bellaveglia, M. Castellano, D. Di Giovenale, G. Di Pirro, M. Ferrario, *et al.*, Nature communications **7** (2016).

[3] C. Behrens, F.-J. Decker, Y. Ding, V. Dolgashev, J. Frisch, Z. Huang, P. Krejcik, H. Loos, A. Lutman, T. Maxwell, *et al.*, Nature communications **5** (2014).

[4] E. Chiadroni, M. Bellaveglia, P. Calvani, M. Castellano, L. Catani, A. Cianchi, G. D. Pirro, M. Ferrario, G. Gatti, O. Limaj, S. Lupi, B. Marchetti, A. Mostacci, E. Pace, L. Palumbo, C. Ronsivalle, R. Pompili, and C. Vaccarezza, Review of Scientific Instruments **84**, 022703 (2013).

[5] N. Matlis, G. Plateau, J. van Tilborg, and W. Leemans, JOSA B **28**, 23 (2011).

[6] S. Wesch, B. Schmidt, C. Behrens, H. Delsim-Hashemi, and P. Schmüser, Nuclear Instruments and Methods in Physics Research Section A: Accelerators, Spectrometers, Detectors and Associated Equipment **665**, 40 (2011).

[7] J. D. Jackson, *Classical Electrodynamics, 3rd Edition, by John David Jackson, pp. 832. ISBN 0-471-30932-X. Wiley-VCH , July 1998.* (John Wiley & Sons, 1998).

[8] V. L. Ginzburg, Physics-Uspekhi **39**, 973 (1996).

[9] K. Bane, F.-J. Decker, Y. Ding, D. Dowell, P. Emma, J. Frisch, Z. Huang, R. Iverson, C. Limborg-Deprey, H. Loos, *et al.*, Physical Review Special Topics-Accelerators and Beams **12**, 030704 (2009).

[10] F. Giorgianni, M. P. Anania, M. Bellaveglia, A. Biagioni, E. Chiadroni, A. Cianchi, M. Daniele, M. Del Franco, D. Di Giovenale, G. Di Pirro, *et al.*, Applied Sciences **6**, 56 (2016).

[11] M. Castellano, V. Verzilov, L. Catani, A. Cianchi, G. Orlandi, and M. Geitz, Physical Review E **63**, 056501 (2001).

[12] A. Cianchi, M. Castellano, L. Catani, E. Chiadroni, K. Honkavaara, and G. Kube, Physical Review Special Topics-Accelerators and Beams **14**, 102803 (2011).

[13] S. Korbly, A. Kesar, J. Sirigiri, and R. Temkin, Physical review letters **94**, 054803 (2005).

[14] M. Shevelev, H. Deng, A. Potylitsyn, G. Naumenko, J. Zhang, S. Lu, S. Gogolev, and D. Shkitov, in *Journal of Physics: Conference Series*, Vol. 357-1 (IOP Publishing, 2012) p. 012023.

[15] V. Verzilov, Physics Letters A **273**, 135 (2000).

[16] I. Wilke, A. M. MacLeod, W. Gillespie, G. Berden, G. Knippels, and A. Van Der Meer, Physical review letters **88**, 124801 (2002).

[17] M. Ferrario, D. Alesini, M. Anania, A. Bacci, M. Bellaveglia, O. Bogdanov, R. Boni, M. Castellano, E. Chiadroni, A. Cianchi, *et al.*, Nuclear Instruments and Methods in Physics Research Section B: Beam Interactions with Materials and Atoms (2013).

[18] M. Ferrario, D. Alesini, A. Bacci, M. Bellaveglia, R. Boni, M. Boscolo, M. Castellano, L. Catani, E. Chiadroni, S. Cialdi, *et al.*, Physical review letters **99**, 234801 (2007).

[19] D. Alesini *et al.*, Nuclear Instruments and Methods in Physics Research Section A: Accelerators, Spectrometers, Detectors and Associated Equipment **507**, 345 (2003).

[20] M. Castellano, V. Verzilov, L. Catani, A. Cianchi, G. D'Auria, M. Ferianis, and C. Rossi, Phys. Rev. E **67**, 015501 (2003).

[21] A. Curcio, M. Anania, F. Bisesto, M. Botton, M. Castellano, E. Chiadroni, A. Cianchi, M. Ferrario, M. Galletti, D. Giulietti, *et al.*, Physical Review Applied **9**, 024004 (2018).

[22] A. Cianchi, D. Alesini, A. Bacci, M. Bellaveglia, R. Boni, M. Boscolo, M. Castellano, L. Catani, E. Chiadroni, S. Cialdi, *et al.*, Physical Review Special Topics-Accelerators and Beams **11**, 032801 (2008).

[23] M. Ferrario, D. Alesini, A. Bacci, M. Bellaveglia, R. Boni, M. Boscolo, P. Calvani, M. Castellano, E. Chiadroni, A. Cianchi, L. Cultrera, G. di Pirro, L. Ficcadenti, D. Filippetto, A. Gallo, G. Gatti, L. Giannessi, M. Labat, S. Lupi, B. Marchetti, C. Marrelli, M. Migliorati, A. Mostacci, D. Nicoletti, E. Pace, L. Palumbo, V. Petrillo, M. Quattromini, C. Ronsivalle, A. R. Rossi, J. Rosenzweig, L. Serafini, M. Serluca, B. Spataro, H. Tomizawa, C. Vaccarezza, and C. Vicario, Nuclear Instruments and Methods in Physics Research A **637**, 43 (2011).

[24] L. Serafini and M. Ferrario, in *American Institute of Physics Conference Series*, Vol. 581 (2001) pp. 87–106.

[25] A. L. Cavalieri, D. Fritz, S. Lee, P. Bucksbaum, D. Reis, J. Rudati, D. Mills, P. Fuoss, G. Stephenson, C. Kao, *et al.*, Physical review letters **94**, 114801 (2005).

[26] R. Pompili, M. Anania, M. Bellaveglia, A. Biagioni, G. Castorina, E. Chiadroni, A. Cianchi, M. Croia, D. Di Giovenale, M. Ferrario, *et al.*, New Journal of Physics **18**, 083033 (2016).

[27] A. Cianchi, D. Alesini, M. Anania, A. Bacci, M. Bellaveglia, M. Castellano, E. Chiadroni, D. Di Giovenale, G. Di Pirro, M. Ferrario, *et al.*, Physical Review Special Topics-Accelerators and Beams **18**, 082804 (2015).

[28] R. Pompili, M. Anania, F. Bisesto, M. Botton, M. Castellano, E. Chiadroni, A. Cianchi, A. Curcio, M. Ferrario, M. Galletti, Z. Henis, M. Petrarca, E. Schleifer, and A. Zigler, Opt. Express **24**, 29512 (2016).